MSc in Photonics
Universitat Politècnica de Catalunya (UPC)
Universitat Autònoma de Barcelona (UAB)
Universitat de Barcelona (UB)
Institut de Ciències Fotòniques (ICFO)
http://www.photonicsbcn.eu

Master in Photonics

MASTER THESIS WORK

TOWARDS CAVITY-ENHANCED DETECTION OF SINGLE IONS IN THE SOLID STATE

Céline Hélène Ida van Valkenhoef

Supervised by Prof. Hugues de Riedmatten, ICFO
Co-supervised by Dr. Bernardo Casabone, ICFO

Presented on the date 6th September 2018

Registered at
Escola Tècnica Superior d'Enginyeria de Telecomunicació de Barcelona

Towards cavity-enhanced detection of single ions in the solid state

Céline Hélène Ida van Valkenhoef
Quantum Photonics with Solids and Atoms group, The Institute of Photonic Sciences (ICFO),
Avenida Carl Friedrich Gauss 3, 08860 Castelldefels, Barcelona, Spain
E-mail: celine.vanvalkenhoef@icfo.eu

Abstract: The goal of this master thesis was to take initial steps towards cavity-enhanced detection of single rare-earth ions in the solid state. A fibre microcavity set-up for use with Praseodymium-doped nanocrystals was designed, built and characterised with light at 606 nm, with the aim to achieve Purcell enhancement. The cavity has a finesse of 3374, linewidth of 14 GHz and FSR of 80 THz. In addition, fluorescence and linewidth measurements of Er^{3+}:Y_2O_3 nanocrystals at room temperature were taken in the telecom range. A primary fluorescence peak at 1535.424 nm with FWHM of 171 GHz was observed, corresponding to the Er^{3+}:$^4I_{13/2} - {}^4I_{15/2}$ transition, and a secondary peak at 1536.851 nm. A population decay time T_1 of 13.3 ms was measured.

Keywords: Cavity-enhanced detection, Purcell effect, Spectroscopy, Er^{3+}:Y_2O_3

1. Introduction

The long-term goal for quantum information science is the development of a quantum web, sharing information with quantum devices via coherence and entanglement through quantum networks [1]. Quantum networks comprise quantum nodes, where quantum information can be generated, processed and stored, with quantum channels linking the nodes [2]. Matter can be used to store and process information, and light can be used to transport information. Therefore, quantum nodes require an efficient interface between quantum light and matter[3]. Single atoms or ions can be used as quantum nodes. However, the interaction between single atoms and single photons in free space is usually quite weak[4]. Different approaches to increasing this light-matter interactions are being investigated, such as using ensembles of atoms and inserting single atoms in high-finesse cavities, in the regime of cavity quantum electrodynamics (CQED). Over the last decades, CQED first studied single atoms. More recently, solid-state systems such as quantum dots and vacancy centres in diamonds [5] were studied, and later on single rare-earth ions [6].

Rare-earth elements or lanthanides are characterised by having a partially filled 4f shell shielded by electrons in the 5s and 5p shells. Although 4f-4f transitions in single rare earth ions are dipole-forbidden, they are weakly probable if the ions are in a solid matrix. The shielding makes the rare earth element's 4f-shell transitions less sensitive to their environments, resulting in properties such as long-lived nuclear spin coherence lifetimes and optical coherence lifetimes. This makes them good candidates for quantum memories [3,7]. Up to now, rare-earth doped crystals have been used mostly with ensemble of ions. However, detecting and manipulating single rare earth ions would enable new possibilities, including the ability to manipulate interactions between different spin qubit, thus implementing quantum gates. The combination of quantum logic and efficient connection with photons would make single rare-earth ions interesting quantum nodes. Praseodymium (Pr) and Erbium (Er) are both rare-earth elements that commonly occur in the 3+ ionisation state. Er^{3+} has a transition in the telecom range at 1535 nm, which is ideal for long-distance quantum communication applications, whilst Pr^{3+} has a transition in the optical range at 619 nm and long-lived spin states, which allow efficient initialisation and manipulation of qubits. Whilst the 4f-4f transitions are only weakly probable, the spontaneous emission can be enhanced through the so-called Purcell effect by coupling the emitter to a cavity [8,9,10]. Recently, first experiments showing cavity-enhanced detection of single rare-earth ions have been performed in nanophotonic cavities [11,12]. In our group, we investigate a different approach based on fibre-based microcavities, which have the advantage of being more flexible and easily tuneable.

The proposal for this master thesis initially had the following objectives: (1) Design and construction of a fibre microcavity set-up for Pr ions optimised for use in cryogenic environment. (2) Stabilisation and characterisation of the fibre cavity. (3) Fabrication of nanocrystals samples. (4)

Cavity-enhanced detection of Pr ions at room temperature with the goal of demonstrating Purcell enhancement, and comparison with theoretical models. Due to a delay in the delivery of the equipment to generate light at 619 nm for the resonant 4f-4f transition excitation of Pr^{3+}, objectives (3) and (4) were not carried out. Instead, spectroscopy of Er^{3+} ceramics and nanocrystal powder at room temperature was carried out and analysed. Due to a delay in testing another microcavity set-up for Erbium ions in a cryogenic environment (built by a PhD-student in the group), there was no feedback to inform about potential design improvements. Therefore it was decided to design the microcavity for this thesis for use at room temperature. The revised objectives are thus: (1) Design and construction of the fibre microcavity set-up for Praseodymium ions for use at room temperature. (2) Stabilisation and characterisation of the fibre cavity. (3) Linewidth and lifetime measurements of Er^{3+} nanocrystals with resonant excitation of the 4f-4f transition at room temperature.

This master thesis is organised as follows. In section 2, I will set out the relevant CQED theory, followed by the design and characterisation of my positioner and fibre microcavity. In section 3, I will discuss the properties of Er^{3+} and Pr^{3+} and the set-up, results and analysis of the Er^{3+} measurements I took. I will then make some concluding remarks.

2. Design, construction and characterisation of the fibre microcavity set-up

2.1. Theoretical background

In this project, I consider a fibre-based Fabry-Pérot cavity (FFPC) consisting of fibre tip that is laser-machined with a concave depression covered with a dielectric coating, thus forming a curved mirror, and a plane mirror, building on the work carried out by David Hunger's group[13]. The rare-earth ions embedded in nanocrystals will eventually be attached to the plane mirror. Figure 1 shows a schematic drawing of such a cavity, with the two mirrors and orange light exciting the purple rare-earth ions.

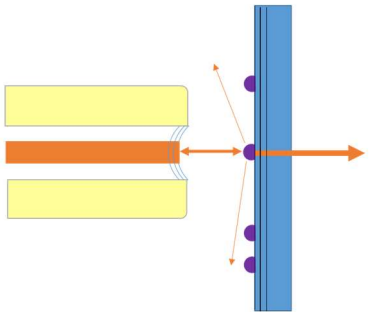

Figure 1. Schematic drawing of Fabry-Pérot cavity

The aim of placing the rare-earth ions in the cavity is to enhance the spontaneous emission rate. This effect can be quantified by the Purcell factor. The following parameters are considered for determining the Purcell factor and to characterise the cavity: [13,14]

- Optical distance between the mirrors L, which includes the penetration of the light into the outer layers of the mirrors
- Free spectral range (FSR) of a cavity is the frequency difference between resonator modes:
  $FSR_\nu = {}^{c}/_{2L}$ (1)
  When scanning the cavity length, the distance between two resonance peaks equals $\lambda/2$. (2)
- Finesse depends on the roundtrip losses, where low losses give a high finesse:
  $$\mathcal{F} = \frac{2\pi}{total\ losses\ per\ roundtrip}$$ (3)
  This can also be defined as: $\mathcal{F} = {}^{\frac{\lambda}{2}}/_{\delta L}$, where δL is the width of the spectral line of the cavity resonator mode when scanning the length of the cavity (4)
- The cavity linewidth $\delta\nu$, typically measured as the full width at half maximum (FWHM) of the TEM_{00} cavity resonances. It can be defined as:
  $$\delta\nu = \frac{total\ losses\ per\ roundtrip}{roundtrip\ duration} = \frac{FSR}{\mathcal{F}} = \frac{c}{2L\mathcal{F}}$$ (5)
- Quality factor
  $Q = {}^{\nu_0}/_{\delta\nu}$, where ν_0 is the resonance frequency (6)
- Waist radius ω_0, which for short cavities with mirrors with very different radii of curvature (ROCs) is determined by the smaller one. For the set-up under discussion, this is the fibre mirror's ROC indicated by R_1. Then:

$$\omega_0 \approx \sqrt{\frac{\lambda}{\pi}}(LR_1)^{1/4} \quad (7)$$

- Mode volume V_m of a cavity is determined by the area of the mode and the cavity length. The minimal cavity length of a FFPC is obtained when the mirrors touch and is therefore determined by the radius of curvature of the fibre mirror.

$$V_m = \frac{\pi}{4}\omega_0^2 L \quad (8)$$

Having defined these parameters, I can now define the Purcell factor and a related parameter.

- The Purcell factor F_P is:

$$F_P = \frac{3Q\left(\lambda/n\right)^3}{4\pi^2 V_m} \quad (9)$$

  Where λ is the free-space wavelength of the light and n is the refractive index of the material inside the cavity. If the Purcell factor $F_P>1$, the spontaneous emission rate is enhanced. The aim of the cavity is to obtain a Purcell factor $F_P>>1$.

- The spontaneous emission coupling factor β gives the fraction of the number of photons that are emitted into the cavity mode with respect to the total number of emitted photons.

$$\beta = \frac{F_P}{F_P+1} \quad (10)$$

  Ideally, the cavity would only emit photons into the cavity mode, and therefore β would approach 1. In practice, there is always some emission into other modes.

It can be seen from the equations that to achieve a high Purcell factor, a high Q value and a small mode volume V_m are required. In addition, the frequencies of the cavity mode and the atomic transition should be close. Thus in designing the cavity, a high finesse and a small mode volume should be aimed for. A high finesse can be achieved by reducing roundtrip losses, e.g. by using high-reflectivity mirrors and minimising intra-cavity loss. To ensure that the cavity mode and the atomic transition are close in frequency, the light used should be resonant with the atomic transition and the cavity length adjusted to multiple of its wavelength. Thus the design should include a mechanism to adjust the cavity length. However, this must not compromise the stability of the cavity. To ensure that resonance is maintained so interaction between photons and atoms can take place, the cavity should be sufficiently stable for a time duration comparable to the emission lifetime. For a cavity with a large enough finesse (~10,000) as I will use in this thesis work, $\lambda/\mathcal{F}$ can be as small as picometres. The cavity therefore has to remain stable for a duration of μs to ms to the order for picometres. As it is intended to place the ion-doped nanocrystals on the planar mirror, the design should also include a mechanism to scan the mirror in order to locate the ions.

2.2. Design and construction

The design of the positioner was made using Inventor, as shown in figure 2(a). It builds on the design invented in the group of Prof. David Hunger. The positioner comprises the following parts: a main block (pink) to which all the components are attached; an arm (yellow) to guide the fibre; a mirror holder (light and dark blue); two motors fixed to the block by blue holders to move the mirror in the x and y-directions; and three piezoelectric actuators (PEAs) (purple) for the steering of the fibre in the x, y and z-directions. The motors can therefore be used to locate and set a region of interest on the mirror. Then the PEAs can be used to move the fibre to locate the nanocrystals within that region of interest. The stability of the arm and the mirror holder are essential for the creation of a stable cavity. Therefore, the mirror holder is held in place by a spring that traverses the block diagonally and the semi-rigid arm is fixed to the main block. As the stress analysis in figure 2(b) shows, the bulk of the arm is rigid, but there is some movement possible at the end shown in red, where the fibre is fed through. This allows small, controlled movements of the fibre in the y and z-directions by the applied force of the PEAs to the arm. Movement of the fibre in the x-directions occurs by a PEA applying force directly to the fibre.

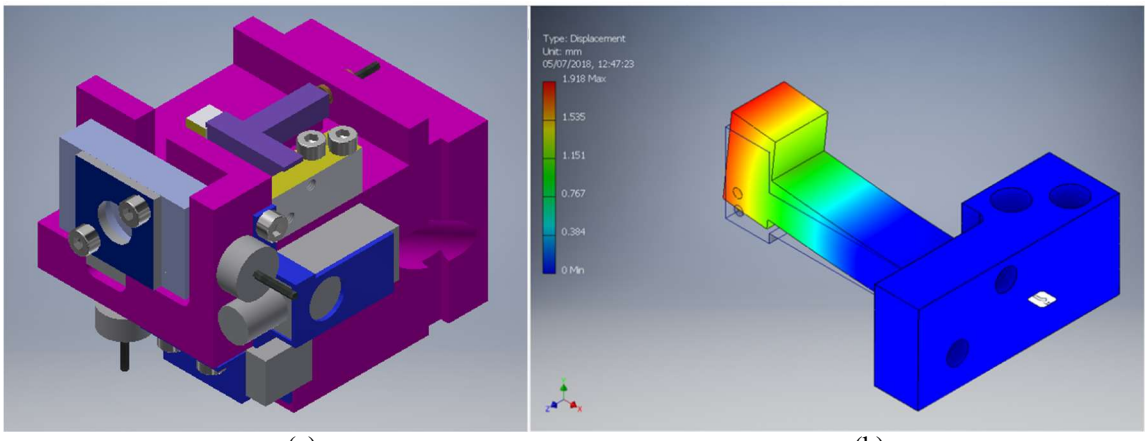

(a) (b)

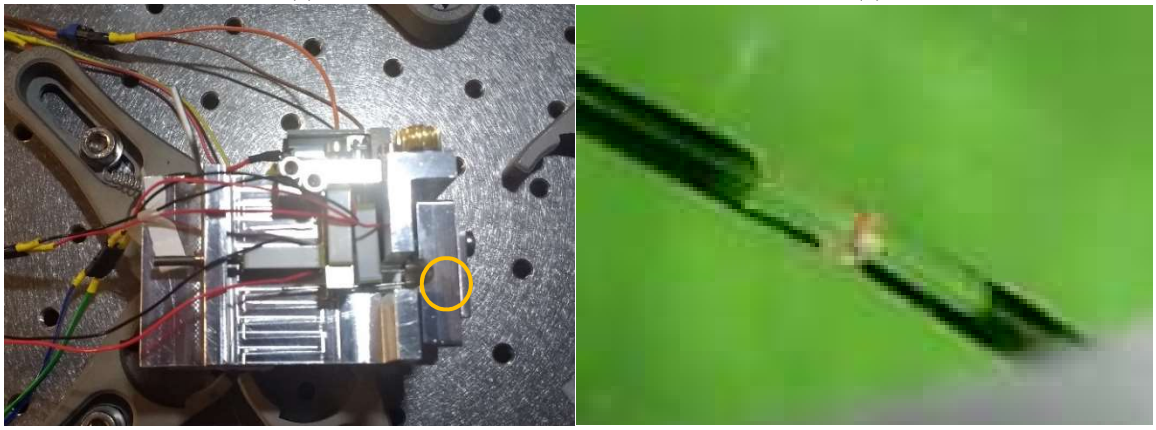

(c) (d)

Figure 2. Design and construction of the positioner, where (a) shows the design in Inventor, (b) shows the stress analysis of the arm through which the fibre is steered, (c) shows a top view of the built positioner; the cavity is located in the yellow circle (but not visible in this photograph) and (d) shows the fibre tip and its reflection, with the actual cavity between the fibre tip and planar mirror.

I re-use a single-mode fibre and mirrors that are optimised for use at 580 nm. It is expected they still will have good reflectivity around 606 and 619 nm. A concave profile has been machined on the fibre tip with a mirror deposited on top. The concave depression has ROC of 51.3 μm and depth of 1.87 μm. Both the mirror that is deposited on the concave depression and the planar mirror have absorption losses of 10 ppm. The fibre was machined by Franziska Beck in the group of Prof. Dr. D. Hunger at the Karslruher Institut fur Technologie.

Scanning of the mirror occurs through the control of coarse movement of the mirror via the motors and fine movement of the arm and fibre via the PEAs. The movement of the mirror holder and the fibre is controlled through the mechanism shown in figure 3. A National Instruments data acquisition card (NIDAQ) controls both the motors and the PEAs in the x and y-directions. The NIDAQ is connected to the motor controllers via digital I/O ports, allowing bidirectional movement of the mirror holder. The NIDAQ is connected to the amplifiers via analogue I/O ports, thus controlling the high voltage input that the PEAs require.

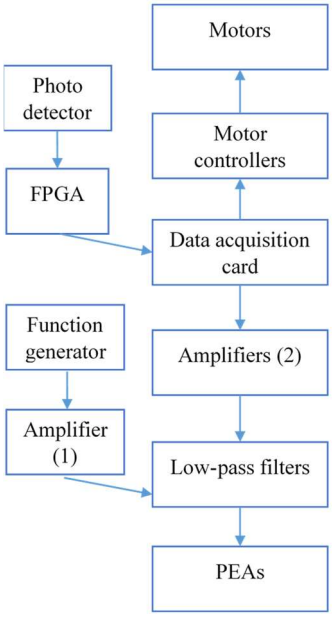

Figure 3. Movement-control set-up.

This allows the positioner to scan an area of the mirror of approximately 50x50 μm to look for the single ions. Movement in the z-direction is controlled by having the relevant PEA controlled by a function generator. Thus a two-dimensional grid is created, where at each position, the cavity is

scanned in the z-direction and data is collected with an avalanche photodetector (APD) of the light transmitted through the planar mirror. If a particle is present at a grid position, I expect to see reduced transmission through the mirror, and thus record lower intensity. The APD is connected to the NIDAQ via a field-programmable gate array (FPGA). The FGPA provides increased processing power compared to the NIDAQ. This allows the FPGA to process the intensity data at each grid position for the cavity scan in the z-direction, for which the NIDAQ does not have a large enough sample rate. It will retain each transmission peak for 16 μs, only discarding it if within that time frame a larger peak is detected. The FPGA will then feedback the processed data to the NIDAQ, which will plot the transmission peak at that grid position. By repeating this for each grid position, a map is created showing the location of any particles present.

2.3. Cavity characterisation

To determine the finesse of the cavity, I obtained the FSR and the cavity linewidth. As the intention is to eventually use the cavity with Pr^{3+}:Y_2O_3 at a wavelength of 619 nm, light of 606 nm is used for its characterisation as this is readily available in our laboratory. The light is coupled into the cavity. The emitted light that passes through the planar mirror is detected by an APD. The fibre tip is moved until it touches the planar mirror, so that the smallest possible cavity is created (length L=1.87μm). Then using a function generator to control the z-axis PEA, the cavity length is scanned by moving the fibre in the z-direction using a triangular wave with a frequency of 20 Hz and amplitude of 0.330V. The trace of the APD measurements shows 0th and higher-order longitudinal modes, as shown in figure 4(a).

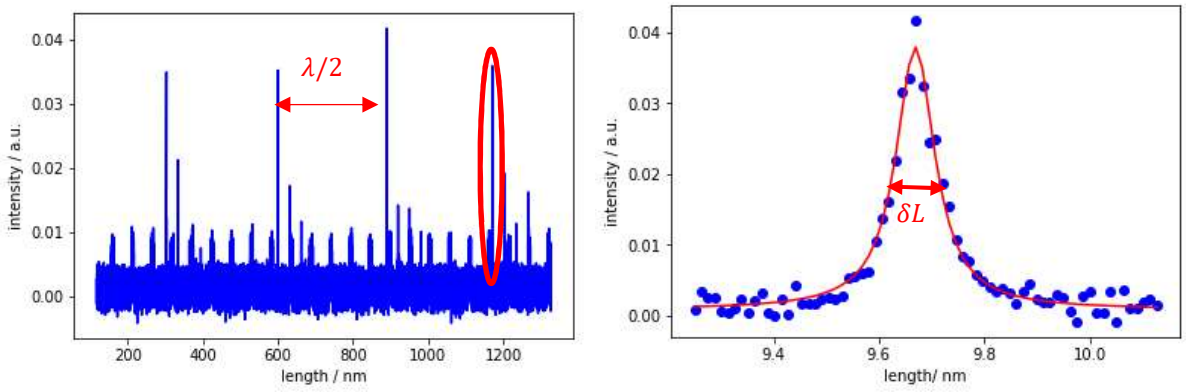

(a) (b)

Figure 4. Cavity characterisation, where (a) shows the cavity resonances when the cavity is scanned near the shortest cavity length determined by the depth of the fibre mirror; the FSR is the distance between resonance peaks and (b) shows the curve fitted to the encircled peak in (a); with the width of the spectral line indicated.

The horizontal axis is calibrated, knowing that the distance between two peaks, the free spectral range, is given by half the wavelength of the light (303 nm). The width of the spectral line δL can be determined using a Lorentzian curve fitting. For the curve fitting, I use a Lorentzian of form $y = \frac{A}{\pi}\frac{{}^{1}/_{2\sigma}}{(x-c)^2+({}^{1}/_{2\sigma})^2} + d$ using Non-Linear Least-Square Minimization and Curve-Fitting (LMFIT) for Python. Then $\delta\lambda$ is given by the FWHM of this curve, which is 0.0898 nm +/- 0.0037 nm.

Using equations 2 and 4, FSR = $\lambda/2$= 303nm, and I obtain a finesse of 3374. For light of wavelength 619 nm, I expect a slightly lower finesse, as it the wavelength is further away from the centre of the reflective coating. Using equation 5 and the cavity length as given by the depth of the concave mirror plus the distance from the shortest cavity length to the analysed resonant mode ($4\lambda/2$), I obtain a cavity linewidth of approximately 14 GHz and an FSR of approximately 80 THz. Using the depth and ROC of the fibre mirror, and equations 7 and 8, I obtain the waist radius and mode volume: $\omega_0 \approx 1374\ nm^2$ and $V_m \approx 2.77\ \mu m^3$. Then using these outcomes with equations 6 and 9, the expected Purcell factor for the shortest possible cavity with this set-up using light of

wavelength 606 nm in free space is 678, which is much larger than 1 as required. Next steps for testing the set-up are described in the conclusion.

3. Er^{3+} spectroscopy

An important task towards the detection and manipulation of single rare-earth ions is to determine the spectroscopic properties of the ions in nanocrystals, such as optical linewidth and population lifetime of the excited state (T_1). In our laboratory, we are currently investigating two ion species as possible candidates for single ion detection, Er^{3+} and Pr^{3+} ions. A PhD student in the group is investigating Er^{3+} ions and has performed spectroscopic measurements on Er^{3+}:Y_2O_3 ceramics. As mentioned previously, the original goal of this master thesis was to start investigating Pr^{3+} ions, but due to a delay in obtaining the required laser source, this could not be done. Instead, I have studied the optical spectroscopic properties of Er^{3+}:Y_2O_3 nanocrystals at room temperature (optical linewidth, population lifetime of the optical transition) and compared it with the results obtained in the ceramic.

3.1. Comparison between Pr^{3+} and Er^{3+} properties

Figure 5 shows the Dieke diagram of the lower energy levels of Er^{3+} and Pr^{3+}[15. The transitions of interest are Er^{3+}:$^4I_{13/2}$ – $^4I_{15/2}$, which has a wavelength of 1535 nm in Er^{3+}:Y_2O_3, and Pr^{3+}:$^3H_4$ – $^1D_2$, which has a wavelength of 619 nm in Pr^{3+}:Y_2O_3. The ground states have hyperfine or Zeeman splitting, which is not shown in this figure.

The Er^{3+}:$^4I_{13/2}$-$^4I_{15/2}$ transition falls in the telecom range, thus making it a good candidate for the transmission of quantum information over long distances in optical fibres. The Pr^{3+}:$^1D_2$-$^3H_4$ transition falls in the optical range. The advantage of using this transition is that it has a short optical lifetime and relatively long spin lifetime. The short optical lifetime leads to a larger repetition rate of experiments for information transfer. The relatively long spin lifetime allows for qubit initialisation and manipulation that is more efficient.

As can be seen from the graph, the spacing of the energy levels of Erbium is much higher than that of Praseodymium, with the latter having many different energy levels between the excited and ground levels of the transition of interest, compared to none in Erbium. This leads to very different branching ratios: 3% for Pr^{3+}:$^3H_4$ – $^1D_2$ and around 20% for Er^{3+}:$^4I_{13/2}$ – $^4I_{15/2}$. This makes the Erbium transition much more efficient than the Praseodymium transition.

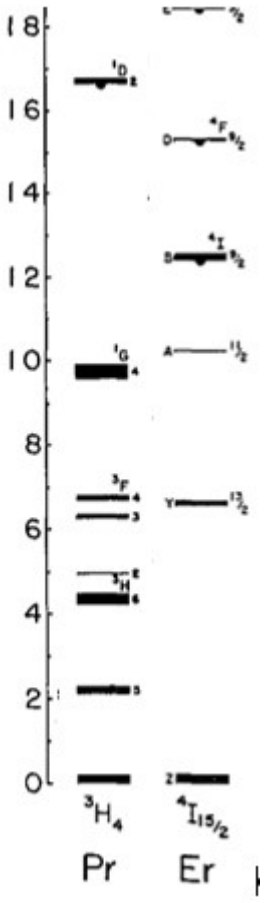

Figure 5. Lower energy levels for Praseodymium and Erbium

3.2. Linewidth and lifetime

The spectral lineshape function of an atomic transition has a characteristic peak that is centred on the energy difference of the atomic transition. An important parameter of the lineshape function is the FWHM, which represents the spectral line broadening of the transition.

In a gas, the main causes of broadening are lifetime broadening due to the uncertainty principle, collisional broadening and Doppler broadening. In a solid-state structure such as Er^{3+}:Y_2O_3 nanocrystals, collisional and Doppler broadening do not apply.

In the solid state, both homogeneous and inhomogeneous broadening occurs. The homogeneous linewidth is usually not lifetime limited, as there is dephasing due to for example magnetic fluctuations, nuclear spin and interaction with phonons. Inhomogeneous broadening occurs in addition to homogeneous broadening, as each ion sees a different environment.

The optical linewidth can therefore not be used to measure the lifetime directly. Instead, the lifetime can be obtained by fitting an exponential curve to a single fluorescence measurement. At

room temperature, the homogeneous linewidth of the ions is expected to be much larger than the inhomogeneous one.

3.3. Fluorescence and linewidth measurements in Er3+ nanocrystals

Whilst there is a range of spectroscopy data available on Er3+ doped glasses and crystals, there have been much less measurements of Er doped nanocrystals. In particular, I am not aware of measurements of optical linewidth at room temperature. To take the measurements, I use Er^{3+}:Y_2O_3 nanocrystals fabricated in the Institut de Recherche Chimie Paris (group of Dr. Philippe Goldner). First, I used a 0.5% Er^{3+}:Y_2O_3 ceramic, which was fabricated for us by sintering the relevant nanocrystal powder at 1500 ℃. Then, I used a 0.02% powder directly.

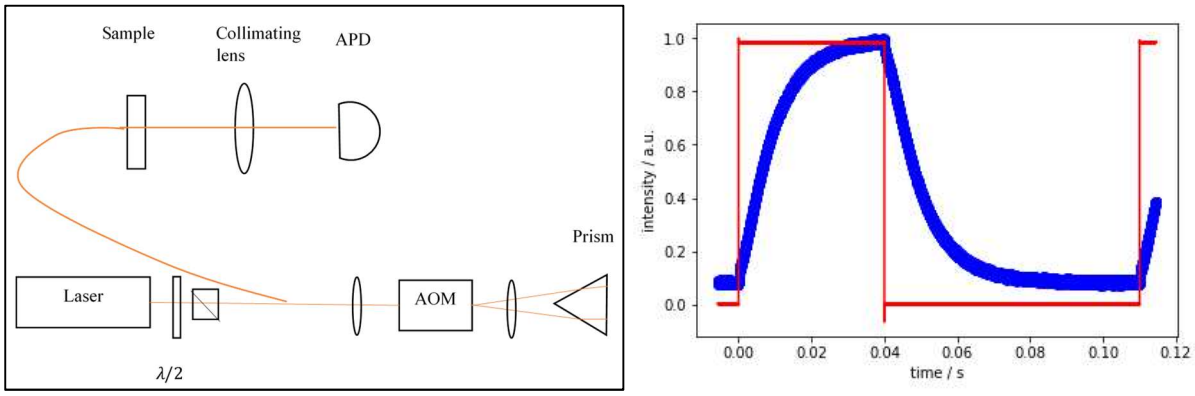

(a) (b)

Figure 6. (a) shows a schematic drawing of measurement set-up and (b) shows an example of a single measurement with the laser pulse in red and the emitted light in blue. Normalisation is carried out, so that the maximum emission equals 1.

Figure 6(a) shows a schematic drawing of the set-up. To reduce laser light directly illuminating the sample, the powder or ceramic was fixed behind a 1 mm diameter hole in an aluminium plate. In order to take measurements free of direct illumination, the laser light was pulsed by putting it through an acousto-optic modulator before directing it to the sample. I used a pulse duration of 40 ms, followed by an off period of 70 ms as shown in figure 6(b). Large collimating lenses collected the emitted light and coupled it into an APD. A tuneable laser was used to take measurements between 1523 and 1550 nm. Initially, I used a step size of 1 nm, with smaller step sizes used close to the centre of the 1535 emission peak. The different step sizes used are summarised in table 1.

Ceramic		**Powder**	
Range / nm	**Step size / nm**	**Range / nm**	**Step size / nm**
1523-1550	1	1523-1550	1
1531.0-1540.0	0.5	1525.0-1545.0	0.5
1533.5-1537.5	0.1	1534.0-1537.0	0.1
1535.00-1536.00	0.05		
1535.35-1535.70	0.01	1535.00-1536.00	0.01
1535.380-1535.470 1535.595-1535.605	0.001		

Table 1: Ranges and step sizes of measurements

For the ceramics, 66 measurements did not return any values due to instrument errors (those at 1535.381 nm and those between 1535.406-1535.470 nm of step size 0.001 nm). For the powder, 11 measurements did not return any values (those between 1535.01 and 1535.12 nm of step size 0.01 nm, with the exception of 1535.10 nm).

Note that I use different wavelengths of light to excite the Er^{3+}. I do not filter the light emitted by the nanocrystals. The plots therefore do not show the amount of light of a certain wavelength that has been emitted, but the amount of light that has been emitted after exciting the nanocrystal at that wavelength.

3.4. Analysis

Figure 7 shows the fluorescence intensity against time for a single measurement of the Erbium illuminated at 1535.470 nm, for the ceramic in (a) and for the nanocrystal powder in (b).

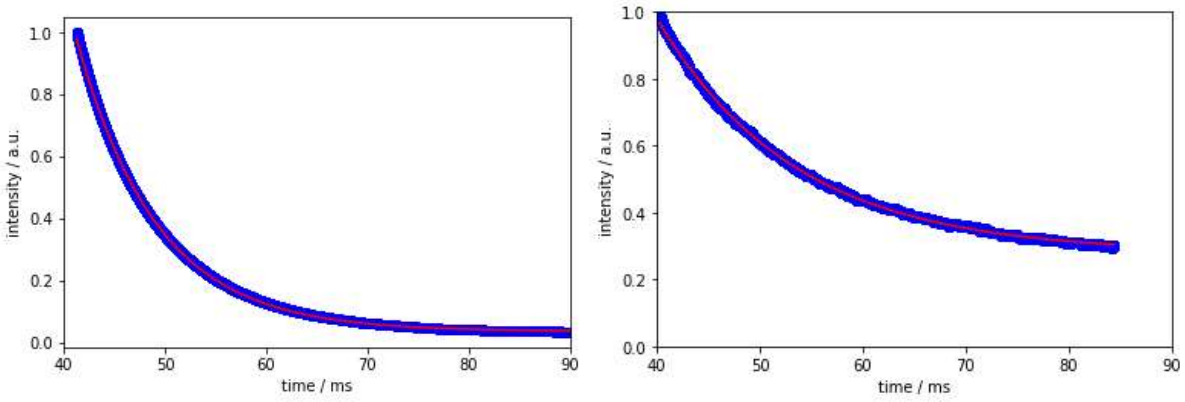

(a) (b)

Figure 7. Lifetime measurements for (a) the ceramic and (b) the nanocrystal powder.

An exponential curve of form $y = A \cdot e^{-x/T1} + d$ is fitted to the data using Non-Linear Least-Square Minimization and Curve-Fitting (LMFIT) for Python. Then T_1 will equate to the 1/e decay time of the fluorescence. This returns the lifetime as 7.89 ms +/- 0.001 ms. I use the same curve fitting for the fluorescence intensity against time for a single measurement of the nanocrystal powder. Here I obtain a lifetime of 13.3 ms +/- 0.003 ms. Therefore there is a large difference between the two measured lifetimes, which is not what I was expecting. The reported lifetime of the $^4I_{13/2} - {}^4I_{15/2}$ transition in bulk crystals $Er^{3+}:Y_2O_3$ is 8.51 ms when Erbium ions are occupying the C_2 crystalographic site [16].

I saw that the intensity of light measured after excitation was much lower for the nanocrystal powder than for the ceramic. This was as I expected, as the nanocrystal powder had a lower concentration of Erbium and the sample was less dense. The fact that the lifetime is much longer in the nanocrystal powder than in the ceramic may also be due to this lower concentration. It could also be caused by the different fabrication process. However, more experiments would be needed to fully explain the difference.

To plot the lineshape function from the measurement data, I use a Python programme to extract 1,000 measured intensities shortly after the laser pulse has terminated for each wavelength I measured and take the average. This equates to a time span of approximately 0.5 ms. I normalise this averaged emission intensity with respect to the laser intensity and plot the intensity against the wavelength. The result of the measurement on the ceramic are shown in figure 8(a). I see a Lorentzian peak just over 1535 nm and a secondary peak around 1537 nm. Curve fitting using a double Lorentzian function L = L1 + L2, where both L1 and L2 are of form $y = \frac{A}{\pi} \cdot \frac{\sigma}{(x-c)^2+\sigma^2}$ using LMFIT shows that the primary peak occurs at 1535.424 nm +/- 0.009 nm, with FWHM 1.349 nm +/- 0.044 nm. This FWHM equates to $\delta\nu$=171 GHz. The secondary peak occurs at 1536.851 nm +/- 0.038 nm and FWHM 1.675 nm +/- 0.165 nm. I use the same methodology to process the measurement data for the nanocrystal powder. Using the same methodology for the curve fitting however does not return a good fit. This suggests that the measurement results do not fit a double Lorentzian shape well. To analyse the results, I use the best-fit parameters from the Erbium ceramic curve fitting for the peaks and FWHMs of the Lorentzians to impose a fit on the nanocrystal powder. I adjust the amplitudes of the two peaks by the same factor and I adjust the offset to account for the differences in measured intensities. I then obtain the curve as shown in figure 8(b). The imposed fit matches the centres of the observed peaks well, so I can conclude that both the ceramic and the nanocrystal powder show fluorescence peaks after having been excited with light of wavelengths 1535.424 and 1536.851 nm.

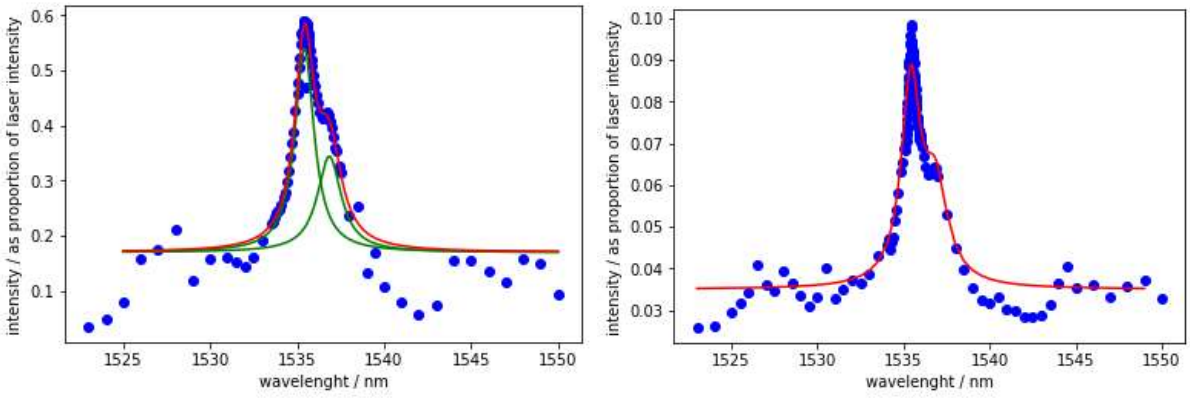

(a) (b)

Figure 8. Measurement data and curve fitting for fluorescence measurements on the Erbium ceramic in (a) and the nanocrystal powder in (b). In (a), the wavelength is plotted against intensity with a double Lorentzian curve fitted in red, which is an addition of the two single Lorentzians shown in green; and in (b), the red curve is the imposed double Lorentzian using best-fit parameters from the graph in (a).

The primary and secondary peaks in the nanocrystal powder have a larger height difference than in the ceramic. This suggests that the FWHM of the secondary peak in the nanocrystal powder is larger than that of the ceramic, and the FWHM of the primary peak in the nanocrystal powder is smaller than that of the ceramic. As noted when discussing the lifetime measurements, there could be a higher level of noise in the nanocrystal powder measurements due to the lower concentration and density of the sample. This could account for the different shape of the graph and the difficulty in fitting a double Lorentzian to the results. Another cause could be that there is some contamination in the nanocrystal powder, giving rise to emission following excitation with a different wavelength near to that of the secondary peak, and thus leading to distortion of the double Lorentzian.

Another interesting feature of the measured lineshapes is the existence of the secondary peak at a distance of 1.43 nm. Within the group, spectroscopy of the Er^{3+}:Y_2O_3 nanocrystals at a temperature of 4K has taken place. The results showed peaks at a similar wavelengths of 1535.4 and 1537 nm. Therefore it can be concluded that the secondary peak is not a result of some measurement error in the measurements taken for this thesis, and neither is the secondary peak a feature that appears at higher temperature only. There remains some discussion about the cause of this secondary peak. The following possibilities were considered:

- The second line could be due to a different Erbium isotope. We discarded this possibility as the isotopic shift is expected to be much smaller.
- The nanocrystals could be a mixture of substitution of the different Y atoms by Erbium in the nanocrystal. However, then the second peak should be at 1545.6 nm, not at 1536.851 nm.[16]. It is interesting to note that in the measurements of both the nanocrystal powder and ceramic, there appears to be a peak around 1545 nm. This indicates that I am using a mixture of Er^{3+}:Y_2O_3 where Er ions are mostly occupying the C_2 site, but a small proportion of ions are occupying the C_{3i} site.
- The secondary peak may be a transition between different crystal field levels. However, as we also observe the secondary peak at low temperatures, this cannot be the case, as at low temperatures, only the lowest crystal field level of the ground state is populated. Additionally, the observed wavelength does not match the crystal field levels.
- The secondary peak may be caused by some contamination or alteration introduced during the production process of the nanocrystals. This would require further investigation.

4. Conclusions

During this thesis project, I have successfully designed, built and characterised a positioner and fibre microcavity. In addition, I have measured and analysed Er^{3+}:Y_2O_3 fluorescence at room temperature, after exciting the sample with light of different wavelengths.

The next steps for the cavity and positioner set-up will be to test if the scanning mechanism successfully locates particles on the mirror. Then a mechanism to lock the cavity should be installed and a mirror prepared with a small amount of Pr^{3+} nanocrystals adhered to it. Once light of wavelength 619 nm has been obtained, cavity-enhanced emission of Pr^{3+} nanocrystals can be attempted. These steps will soon be undertaken by another student.

The Er^{3+}:Y_2O_3 fluorescence measurement results were somewhat unexpected. Firstly, I expected that the excitation would not result in enough emitted light to be detected with an APD. As I was able to do so, the emission was stronger than I expected. Secondly, I detected a secondary peak at 1536.851, which has not been reported in the literature previously. Further consideration should be given to the cause of this peak. Finally, I measured different lifetimes for the nanocrystal powder and ceramic, for which I have identified various possible causes.

Comparing the measured Erbium linewidth of 171 GHz to the cavity linewidth of 14 GHz, shows that the cavity linewidth is clearly much smaller than the linewidth of the Er^{3+}:$^4I_{13/2}$-$^4I_{15/2}$ transition at room temperature. As the cavity linewidth indicates the size of the frequency bandwidth that resonates inside the cavity, and with a large difference in linewidths between Erbium and the cavity, it would be difficult to obtain cavity-enhanced emission at room temperature. As the Erbium linewidth will decrease with decreasing temperature due to a reduction in homogeneous broadening, cavity-enhanced emission should be attempted at low temperature.

Acknowledgements

I would like to thank Hugues, Bernardo and Chetan for their help, advice, explanations and support during the experiment and writing of the thesis, and the whole of the QPSA group for welcoming me into the group.

References

[1] https://qt.eu/about/
[2] Kimble H J 2008 The quantum internet. *Nature* **453** 1023-1030
[3] de Riedmatten H and Afzelius M 2015 Quantum light storage in solid state atomic ensembles in *Engineering the Atom-Photon Interaction* (Springer) 241-273
[4] Kolesov R, Xia K, Reuter R, Stohr R, Zappe A, Meijer J, Hemmer P R, Wrachtrup J 2012 Optical detection of a single rare-earth ion in a crystal *Nature Communications* **3** 1029
[5] Van Dam S, Ruf M, Hanson R 2018 Optimal design of diamond-air microcavities for quantum networks using an analytical approach *arXiv:1806.11474*
[6] Casabone B, Benedikter J, Hummer T, Beck F, Hansch T, Ferrier A, Goldner P, de Riedmatten H, Hunger D 2018 Cavity-enhanced spectroscopy of a few-ion ensemble in Eu3+:Y2O3 a*rXiv:1802.06709*
[7] De Riedmatten H, Afzelius M, Staudt M, Simon C and Gisin N 2008 A solid-state light-matter interface at the single photon level *Nature* **456** 773-777
[8] Kenyon A 2002 Recent developments in rare-earth doped materials for optoelectronics *Progress in Quantum Electronics* **26** 225-284
[9] Eichhammer E, Utikal T, Gotzinger S and Sandoghdar V 2015 High-resolution spectroscopy of single Pr3+ ions on the 3H4-1D2 transition *New Journal of Physics* **17** 083018
[10] Macfarlane R M 2002 High-resolution laser spectroscopy of rare-earth doped insulators: A personal perspective *Journal of Luminescence* **100(1-4)** 1-20
[11] Zhong T, Kindem J, Bartholomew, J G, Rochman J, Craiciu I, Verma V, Nam S W, Marsili F, Shaw M, Beyer A D and Faraon A 2018 Optically addressing single rare-earth ions in a nanophotonic cavity a*rXiv:1803.07520*
[12] Dibos A M, Raha M, Phenicie C M, Thompson J D 2018 Atomic Source of Single Photons in the Telecom Band *Physical Review Letters* **24** 243601
[13] Hunger D, Steinmetz T, Colombe Y, Deutsch C, Hansch T, Reichel J 2010 A fiber Fabry Perot cavity with high finesse *New Journal of Physics* **12** 065038
[14] Fox M 2006 Quantum optics: an introduction (New York: Oxford University Press)
[15] Dieke G, Crosswhite H, Dunn B 1961 *Journal of the Optical Society of America* **51(8)** 820
[16] Reinemer G D 2003 Optical characterization of perturbed sites and C3i sites in rare earth doped oxide crystals A dissertation submitted in partial fulfilment of the requirements for the degree of Doctor of Philosophy in Physics *Montana State University*